Oncogene (2006) 25, 1584–1592

www.nature.com/onc

Parallel induction of ATM-dependent pro- and antiapoptotic signals in response to ionizing radiation in murine lymphoid tissue

S Rashi-Elkeles[1,5], R Elkon[1,5], N Weizman[2], C Linhart[3], N Amariglio[4], G Sternberg[1], G Rechavi[4], A Barzilai[2], R Shamir[3] and Y Shiloh[1]

[1]*The David and Inez Myers Laboratory for Genetic Research, Department of Human Genetics, Sackler School of Medicine, Tel Aviv, Israel;* [2]*Department of Neurobiochemistry, George S Wise Faculty of Life Sciences, Tel Aviv, Israel;* [3]*School of Computer Science, Tel Aviv, Israel and* [4]*Department of Pediatric Hemato-Oncology and Functional Genomics, The Chaim Sheba Medical Center and Sackler School of Medicine, Tel Aviv University, Tel Aviv, Israel*

The ATM protein kinase, functionally missing in patients with the human genetic disorder ataxia-telangiectasia, is a master regulator of the cellular network induced by DNA double-strand breaks. The *ATM* gene is also frequently mutated in sporadic cancers of lymphoid origin. Here, we applied a functional genomics approach that combined gene expression profiling and computational promoter analysis to obtain global dissection of the transcriptional response to ionizing radiation in murine lymphoid tissue. Cluster analysis revealed a prominent pattern characterizing dozens of genes whose response to irradiation was Atm-dependent. Computational analysis identified significant enrichment of the binding site signatures of NF-κB and p53 among promoters of these genes, pointing to the major role of these two transcription factors in mediating the Atm-dependent transcriptional response in the irradiated lymphoid tissue. Examination of the response showed that pro- and antiapoptotic signals were simultaneously induced, with the proapoptotic pathway mediated by p53 targets, and the prosurvival pathway by NF-κB targets. These findings further elucidate the molecular network induced by IR, point to novel putative NF-κB targets, and suggest a mechanistic model for cellular balancing between pro- and antiapoptotic signals induced by IR in lymphoid tissues, which has implications for cancer management. The emerging model suggests that restoring the p53-mediated apoptotic arm while blocking the NF-κB-mediated prosurvival arm could effectively increase the radiosensitivity of lymphoid tumors.
Oncogene (2006) **25,** 1584–1592. doi:10.1038/sj.onc.1209189; published online 28 November 2005

Keywords: ATM; NF-κB; p53; IR response; microarrays

Correspondence: Dr Y Shiloh, The David and Inez Myers Laboratory for Genetic Research, Department of Human Genetics, Sackler School of Medicine, Tel Aviv 66978, Israel.
E-mail: yossih@post.tau.ac.il
[5]These authors contributed equally to this work.
Received 9 August 2005; revised 12 September 2005; accepted 12 September 2005; published online 28 November 2005

Introduction

DNA damage is a major threat to cellular homeostasis and life. The DNA damage response network involves parallel modulation of a wide array of signaling pathways, including lesion processing and repair, activation of cell cycle checkpoints, the apoptotic pathway, and many less characterized stress signals (Shiloh, 2003; Bakkenist and Kastan, 2004). Characterization of gene expression profiles following DNA damage indicated a wider scope of transcriptional response to such damage than previously estimated (Jelinsky and Samson, 1999; Jelinsky *et al*., 2000; Gasch *et al*., 2001).

Regulation of transcription is a key process in physiological networks, being an endpoint of many signal transduction pathways emanating from extracellular and intracellular triggers. DNA microarrays used to analyse transcriptional networks is a mainstay technology in functional genomics (Lockhart and Winzeler, 2000). Construction of gene expression profiles in different physiological conditions identifies the transcriptional programs that are activated under these conditions. Microarray measurements do not, however, directly reveal the regulators of such responses, that is, the transcription factors that control the observed alterations in gene expression. Combining computational promoter analysis with microarray data can elucidate the regulatory layer of transcriptional networks (Tavazoie *et al*., 1999; Jelinsky *et al*., 2000; Elkon *et al*., 2003).

Here, we applied a functional genomics approach that combines genome-scale gene expression profiling with computational promoter analysis to obtain global dissection of the transcriptional response to ionizing radiation (IR) in murine lymphoid tissue, to identify components in this network that are dependent on functional ATM protein, and to reveal major transcription factors that control the induced transcriptional response. The critical cytotoxic DNA lesion inflicted by IR is the DNA double-strand break (DSB). The ATM protein kinase is a master regulator of the cellular response to this DNA lesion (Shiloh, 2003; Kurz and Lees-Miller, 2004). Following DSB induction, ATM is activated and phosphorylates a series of substrates, each

of which is a key component in a certain branch of the DNA damage response network. ATM is missing or inactivated in patients with the autosomal recessive disease ataxia-telangiectasia (A-T). A-T is characterized by cerebellar degeneration, immunodeficiency, genomic instability, cancer predisposition, and extreme sensitivity to IR and radiomimetic chemicals (Chun and Gatti, 2004). A-T cells are defective in the activation of the entire damage response network following DSB induction (Shiloh and Kastan, 2001; Shiloh, 2003). Thus, cells or tissues deficient in ATM are a valuable resource for studying the cellular response to one of the most critical types of DNA lesions.

ATM is frequently mutated in tumors of lymphoid origin (Stankovic *et al*., 2002a), among them the B-cell chronic lymphocytic leukemia (B-CLL) tumors, which are the most common leukemia in western countries. B-CLL tumors that carry mutations in either ATM or p53 are associated with poor clinical course, although ATM-mutant B-CLL tumors are less aggressive than the p53-mutant ones (Pettitt *et al*., 2001; Stankovic *et al*., 2002b). Recently, applying microarray technology, Stankovic *et al*. (2004) showed that the p53-mediated transcriptional response induced by IR is only a subset of the ATM-dependent response. They observed that in addition to the p53-arm, which conveys proapoptotic signals, the ATM-dependent response has a second arm that is enriched with prosurvival signals. This observation suggested an underlying molecular model for the phenotypic difference between ATM- and p53-mutant B-CLL tumors. The regulators that mediated the prosurvival signals remained unknown.

In this study, we recorded genome-wide gene expression profiles in lymph nodes of Atm+/+ and Atm-deficient mice as a representative model for a lymphoid tissue. We observed an Atm-dependent, parallel induction of pro- and antiapoptotic signals in response to IR. Using an advanced computational approach, we revealed that two major transcription factors, NF-κB and p53, mediated the Atm-dependent transcriptional program, with the p53- and the NF-κB-mediated arms inducing pro- and antiapoptotic genes, respectively. Our findings point to novel putative NF-κB targets, and suggest a mechanistic model for cellular balancing between pro- and antiapoptotic signals induced by IR in lymphoid tissues, which have implications for rational drug design and suggest more effective therapeutic targets in the management of leukemias of lymphoid origin.

Results

Expression profiles in irradiated wild-type and Atm-deficient murine lymphoid tissue

Global transcriptional responses were recorded in Atm+/+ and Atm-deficient lymph node tissues of unirradiated mice, and 30 and 120 min after exposure to whole body irradiation with 15 Gy of IR. As a filtering step, we defined the set of 'responding genes', consisting of genes whose expression level was changed by at least 1.75-fold across the tested conditions. Some 10% of the probe sets present in the array, 1206 out of 12 488, met this criterion.

Identification of major expression patterns

Clustering algorithms are a powerful tool for identifying prominent expression patterns obtained from microarray data. These algorithms partition the genes into distinct clusters, each one characterized by a specific expression pattern across the tested conditions. We subjected the set of responding genes to CLICK, a clustering algorithm that yields an optimal balance of intra-cluster homogeneity and inter-cluster separation (Sharan and Shamir, 2000). Prior to clustering, expression levels of each gene were standardized to have a mean value of zero and variance of one; hence, genes clustered together share expression patterns across the tested conditions, but might differ in the magnitude of their response. CLICK identified ten clusters with more than 40 genes. The six major clusters are shown in Figure 1. Clusters 1 and 2 represent Atm-dependent expression patterns: that is, they contain genes that were induced by IR in the Atm+/+ tissue, while their activation in the Atm-deficient tissue was significantly abrogated. Cluster 1 represents 'early responders' that were already transcriptionally activated at the early time point of 30 min post IR, and whose activation was Atm-dependent. Cluster 2 represents a later wave of Atm-dependent genes induction. Clusters 3 and 4 contain genes that were either activated (cluster 3) or repressed (cluster 4) in both genotypes. Clusters 5 and 6 contain genes that responded only in the Atm-deficient tissue. A complete list of the genes contained in these clusters is provided in Supplementary Table A.

Functional categories within gene clusters

Examination of the genes that responded to IR indicated that the network activated following IR spans many biological processes covering most aspects of the cellular physiology. In an attempt to systematically characterize this network, we applied tests aimed at identifying functional categories that are statistically enriched in the clusters. We utilized functional annotations of mouse genes provided by the Mouse Genome Informatics (MGI), which uses the standard vocabulary introduced by the Gene Ontology (GO) consortium (Ashburner *et al*., 2000). Enriched functional categories ($P<0.01$) were identified in four of the clusters (Table 1; list of genes associated with each of the enriched functional categories is provided in Supplementary Table B). Importantly, regulation of cell cycle and apoptosis were among the categories enriched in the Atm-dependent clusters, pointing to their defective activation in the Atm-deficient tissue.

Computational search for mediating transcriptional regulators

We sought to identify transcriptional regulators that control the observed modulation in gene expression

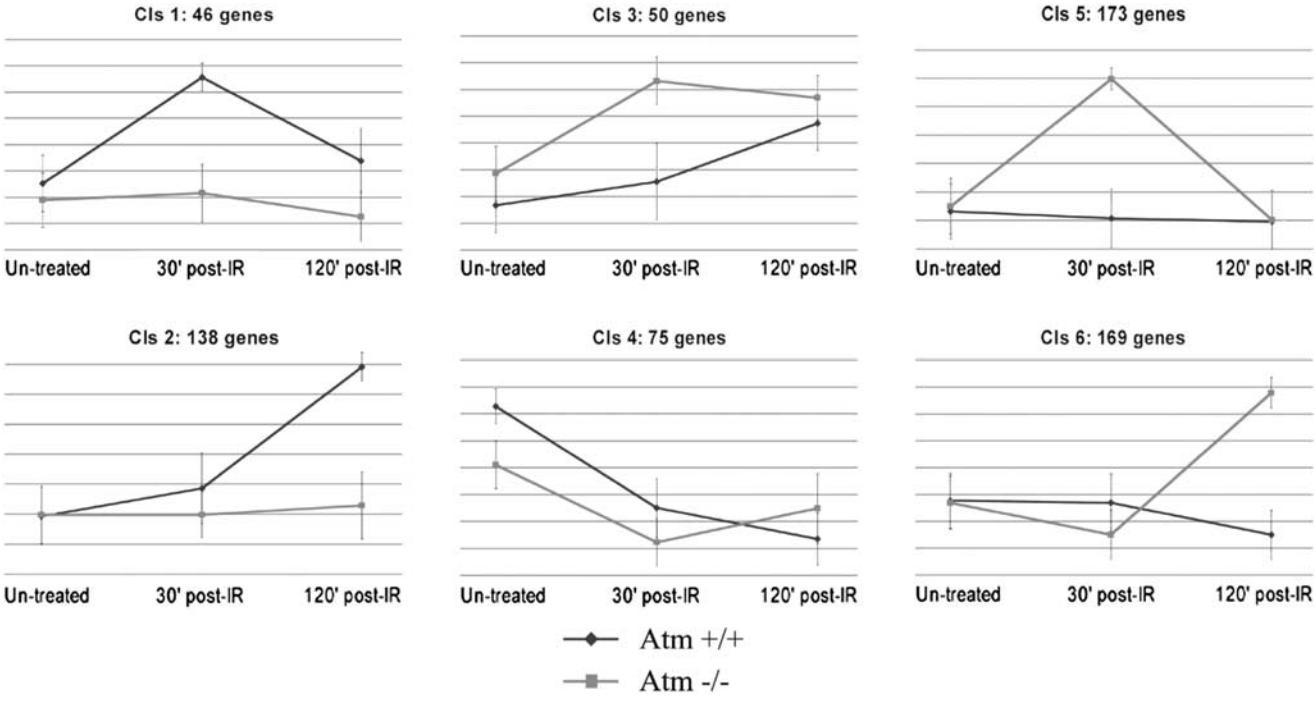

Figure 1 Major clusters identified by CLICK in the set of 1206 responding genes. Each cluster represents a set of genes with similar expression patterns. Prior to clustering, the expression levels of each gene were standardized to have a mean value of 0, and variance of 1. The *y*-axis represents these standardized values. The *x*-axis corresponds to the tested conditions: unirradiated animals, and 30 and 120 min postirradiation. Shown for each cluster is the mean expression pattern calculated over all the genes contained in it, in Atm +/+ (blue) and Atm-deficient tissues (red). Error bars represent one s.d. The total number of genes in each cluster is indicated. Clusters 1 and 2 contain early and late Atm-dependent responders. Clusters 3 and 4 represent genes that exhibited similar response patterns in both genotypes. Clusters 5 and 6 represent early and late responding genes that were activated in Atm-deficient but not in the Atm +/+ tissue. A complete list of genes in each cluster is provided in Supplementary Table A.

Table 1 Enriched functional categories

Cluster	*Number of genes with functional annotations*	*Functional category*	*GO ID*	*Number of genes associated with the category*
1	25	Cell cycle	GO:0007049	7
2	63	Regulation of cell cycle	GO:0000074	7
		Cytokine activity	GO:0005125	5
		Apoptosis	GO:0006915	5
5	83	Electron transport	GO:0006118	8
6	54	Response to pathogen	GO:0009613	13
		Inflammatory response	GO:0006954	6

following IR. We were particularly interested in regulators whose activation is compromised in Atm-deficient tissues. To this end we applied a computational promoter analysis software, we recently developed called PRIMA (PRomotor Integration in Microarray Analysis) (Elkon *et al*., 2003). Based on the assumption that genes that exhibit similar transcriptional expression patterns across multiple conditions share cis-regulatory elements in their promoters, PRIMA seeks out these common sequence elements. In previous work, we demonstrated that PRIMA is sufficiently sensitive to reveal transcription factors (TFs) that control intricate transcriptional networks in human cells (Elkon *et al*., 2003). Given a target set and a background set of promoters, PRIMA performs statistical tests aimed at identifying TFs whose binding site signatures are significantly more prevalent in the target set than in the background set. In this study, each gene cluster was considered a target set and the entire collection of putative murine promoters was the background set (see Materials and methods).

PRIMA identified several TFs whose binding site signatures were significantly overrepresented in cluster 2, which corresponds to the later wave of Atm-dependent gene induction (Table 2). The highest enrichment was observed for NF-κB and p53, which are both well-established stress-induced transcriptional regulators. The incidence of the NF-κB binding

signature was more than fourfold higher among the promoters of cluster 2 than in the background set. This enrichment was robust as it remained solid over a large range of threshold values. Several of the genes in which we identified strong NF-κB binding site signature were previously reported to be under direct control of NF-κB, while the others are novel putative NF-κB targets and require experimental validation (Supplementary Table C). Of note, this set of genes contains subunits of the NF-κB heterodimer itself (Relb, Nfkb2), as well as two of its direct inhibitors, Nfkbia (IκBα) and Nfkbib (IκBβ). This pattern of parallel activation of positive and negative regulators, which probably represents positive and negative feedback loops, appears to be a recurrent theme in the logic of cellular signaling networks. This theme appears in the p53-mediated arm as well, where p53 induces its inhibitor MDM2. PRIMA identified high enrichment for p53 binding site signatures in promoters of this cluster, which was fourfold higher than expected according to the prevalence of p53 hits in the background set (Table 2). p53 binds to a consensus DNA sequence consisting of two conserved decamers separated by a spacer varying in length from 0 to 13 base pairs (el-Deiry *et al*., 1992). The PWM used by PRIMA to represent p53 binding sites does not model the flexibility in the length of the spacer between the decamer repeats, and therefore may have missed possible p53 binding sites in the promoters of this cluster that contain a spacer between the decamers.

Table 2 Transcription factors whose binding site signatures were found by PRIMA to be enriched in promoters of cluster #2

Transcription factor	*Accession number in TRANSFAC DB*	*Enrichment factor*[a]	*P-value*
NF-κB	M00054	4.3	8.0×10^{-9}
p53	M00034	4.2	1.5×10^{-5}
Sp1	M00196	1.6	3.1×10^{-5}
STAT1	M00496	2.9	4.1×10^{-4}

[a]The ratio between the prevalence of transcription factor hits found by PRIMA in promoters of the genes contained in cluster #2 and in promoters of the background set of all mouse promoters.

Real-time RT–PCR validation of microarray data

We performed quantitative real-time RT–PCR analysis of the expression of eleven genes that were induced in an Atm-dependent manner. We focused on the putative NF-κB-mediated arm, since the p53-mediated arm is well-documented. We selected for validation genes whose promoters were found to contain a strong NF-κB binding signature. To reduce the false positive rate, we required that a strong NF-κB binding signature appear also in the promoters of the human ortholog genes. We found good agreement between the microarray and RT–PCR results; the magnitudes of induction differed for some genes but the dependency of their activation on functional Atm was validated for all 11 examined genes (Figure 2).

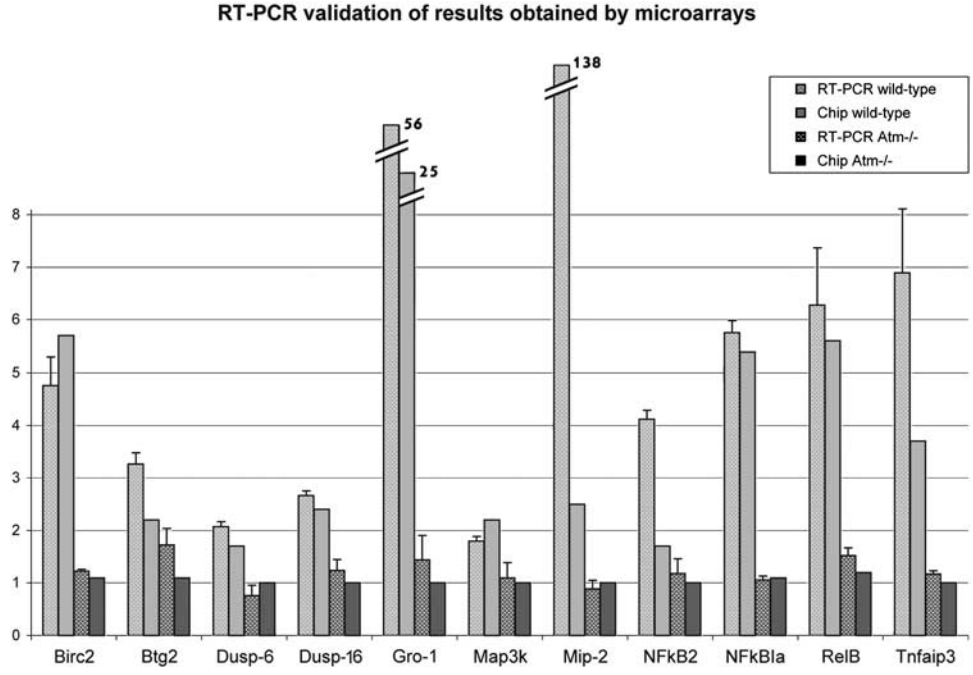

Figure 2 Comparison of gene expression (induction fold) obtained from microarray data and real-time RT–PCR analysis for 11 genes selected from the set of Atm-dependent, putatively NF-κB-mediated responding genes (Supplementary Table C). Four bars are shown for each gene: the blue and red bars represent fold induction of that gene 120 min post IR in the Atm+/+ and Atm-deficient tissues, respectively. Within each genotype, the dotted bar denotes the result obtained by RT–PCR (averaged over three independent measurements, error bars represent one s.d.), and the solid bar denotes the value obtained from microarray measurements. Note that although the magnitude of induction of some genes differs in the real-time RT–PCR and microarray measurements, all 11 genes show agreement between the two technologies on the dependency of the induction on Atm.

Biochemical demonstration of Atm-dependent activation of NF-κB in response to IR

A combination of microarray-based and computational analysis pointed us to the major involvement of NF-κB in Atm-mediated gene regulation in the lymphoid cells following IR. We sought to confirm this phenomenon by direct biochemical demonstration of the dependency of the IR-induced NF-κB activation on Atm. Electromobility shift assays (EMSA) performed on nuclear extracts from lymph node tissues of untreated and irradiated Atm+/+ and Atm-deficient mice showed that while NF-κB binding activity in the Atm+/+ tissue was induced by 2.5-fold following IR, the irradiated Atm-deficient tissue failed to induce NF-κB binding activity (Figure 3). These data demonstrate that the induction of NF-κB in lymphocytic cells in response to IR is indeed Atm-dependent.

Apoptotic signals in the IR-induced transcriptional response

In order to identify biological endpoints of the Atm-dependent gene regulation mediated by NF-κB and p53, we applied a newly developed tool, SHowcase for ATM Related Pathways (SHARP) to our dataset. SHARP is a visualization tool developed in our labs that allows interactive graphic viewing of biological interactions that are stored in a dedicated signaling-pathway database, dynamic navigation through the networks, and superposition of DNA microarray data on the signaling maps (manuscript in preparation). Figure 4, generated using SHARP, indicates that while the p53-regulated arm induced by IR includes two major proapoptotic regulators (Apaf1 and Bax, which are both direct targets of p53 (Miyashita and Reed, 1995; Wang *et al*., 1998; Robles *et al*., 2001)), the NF-κB-mediated arm contains three pivotal antiapoptotic genes (Birc2, Birc3, and TNFaip3, all direct targets of NF-κB (Wang *et al*., 1998; He and Ting, 2002)). Birc2 and Birc3 (cIAP1, cIAP2) are members of the Inhibitor of apoptosis (IAP) family of proteins that inhibit apoptosis probably by directly interfering with activation of several caspases, including Casp3 and 9 (Wang *et al*., 1998; Deveraux and Reed, 1999). Tnfaip3 (A20) was reported to inhibit TNF-induced apoptosis by disrupting the recruitment of TRADD and RIP to the complex that assembles at the TNF receptor shortly after it is bound by its ligand (He and Ting, 2002). Our results show that in response to IR, pro- and antiapoptotic signals are induced in parallel, and the induction of both arms is Atm-dependent. The pro- and antiapoptotic signals were conveyed via direct targets of p53 and NF-κB.

Comparison with IR-induced transcriptional response observed in human B-CLL cells

In a recent study, Stankovic *et al*. (2004) recorded gene expression profiles in ATM-mutant, p53-mutant, and ATM/p53 wild-type B-CLL cancer samples. Similar to the results obtained in our dataset, these authors reported that the ATM-dependent transcriptional

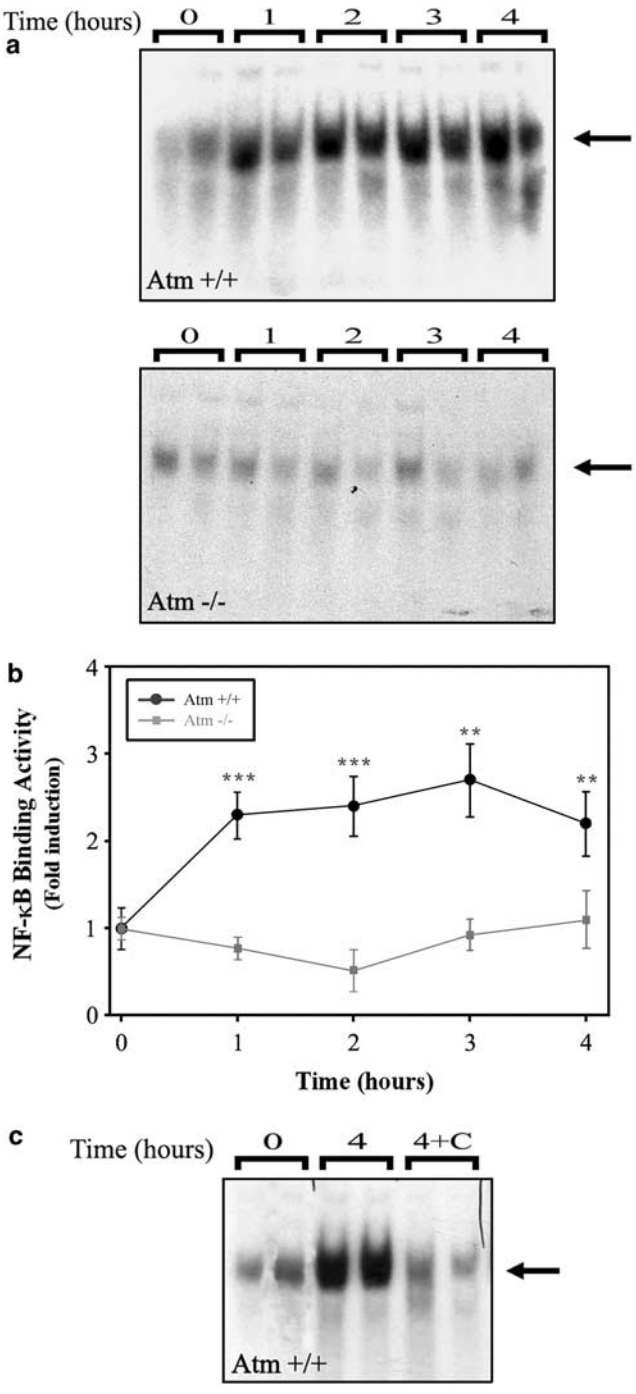

Figure 3 NF-κB binding activity in wild-type and Atm−/− lymphoid tissues following exposure to 20 Gy X-rays. (**a**) EMSA results obtained from two animals are shown for each of the indicated time point. The arrows indicate the position of the NF-κB-DNA complexes. (**b**) Quantitative analysis of NF-κB binding activity fold induction ($n=4$ for each time point). $^{***}P<0.01$; $^{**}P<0.025$. Error bars represent ± s.d. Statistical analyses were performed using two-tailed Student's *t*-test. (**c**) To demonstrate the NF-κB specificity of the shifted bands, nuclear proteins isolated from irradiated Atm+/+ tissues were exposed to 100-fold excess of unlabeled oligonucleotides representing NF-κB-binding consensus sequence, and then incubated with radiolabeled probe (4+C). Band intensity was significantly reduced under this condition.

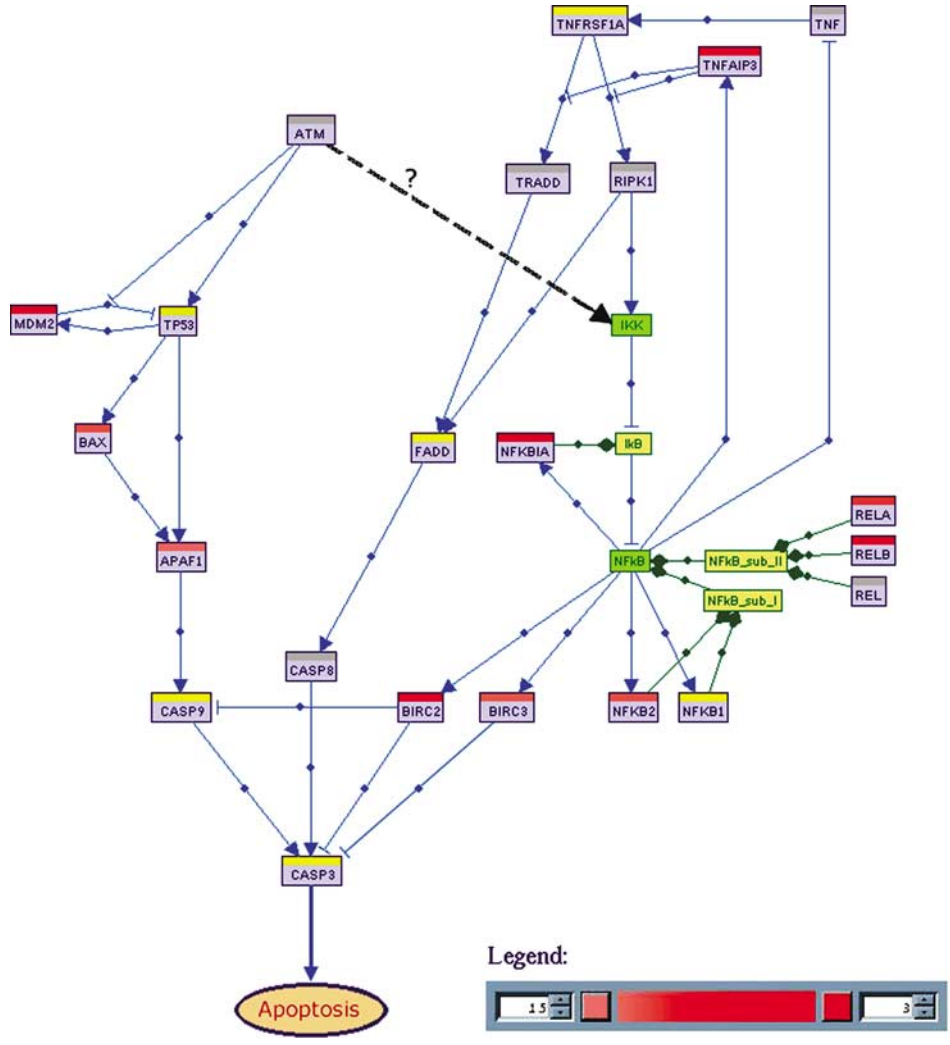

Figure 4 Parallel, Atm-dependent induction of pro- and antiapoptotic signals in response to IR in murine lymphoid tissue. Superposition of microarray results on gene-interaction map points to parallel induction of pro- and antiapoptotic signals, with the proapoptotic pathway mediated by p53 (through its induction of Apaf1 and Bax), and the antiapoptotic arm mediated by NF-κB (through its induction of Birc2, Birc3, and Tnfaip3). The activation of both arms was dependent on Atm in our data set. p53 is a direct substrate of ATM. The mechanism by which ATM activates the NF-κB arm is yet to be determined. The figure was created using SHARP. The interaction map contains nodes of three types: gray nodes represent single proteins (denoted by the official Human Genome Nomenclature Committee (HGNC) symbol of their encoding gene), yellow nodes represent protein families (e.g., IκB), and green nodes represent protein complexes (e.g., IKK); and edges of two types: the first type denotes regulation relations ($\rightarrow$ denotes 'activation', $\dashv$ denotes 'inhibition') and the second type denotes containment relations (green arrows) among nodes (e.g., RelA is contained in NF-κB_subII family). Protein nodes were colored by SHARP according to the fold-induction exhibited by their encoding genes in the Atm+/+ tissue 120 min post-IR: red – induction, green – repression, yellow – no change, gray – data not available (gene was either not present on the microarray or its expression level was below detection limit).

response is composed of two major arms: one is p53-dependent and contains many proapoptotic genes, while the other, controlled by an unknown TF, is enriched with prosurvival genes. In an effort to disclose the regulator of the ATM-dependent, p53-indepndent response observed in that study, we applied PRIMA to the cluster of 61 genes that were reported to respond to IR in the wild type and p53-mutant but not in the ATM-mutant B-CLL tumors. In full concordance with the result obtained on our dataset, we found that the ATM-dependent, p53-independent, prosurvival cluster reported by Stankovic *et al*. (2004) was significantly enriched for NF-κB binding site signature. The prevalence of NF-κB binding site signature on genes' promoters of this cluster was more than fourfold higher than in the background set comprised of all human known-genes' promoters (*P*-value of this over-representation is 4.7×10^{-6}). Notably, similar to findings on our data, this cluster contained several subunits of NF-κB itself (NFKB1, NFKB2, RelB), further supporting a major role for this TF in the induction of this prosurvival transcriptional response.

Discussion

In this study we '*reversed-engineered*' components of the transcriptional network induced by IR in murine lymphoid tissues. Using the microarray technology, we first identified a prominent cluster of genes whose activation by IR was Atm-dependent. We then applied a computational method to search the promoters of these genes for over-represented cis-regulatory elements. Without any bias of prior knowledge, PRIMA revealed highly significant enrichment for NF-κB and p53 binding site signatures, suggesting that these two TFs are the major transcriptional regulators in the Atm-dependent response to IR in lymphoid tissues. These results are in agreement with previous studies that reported compromised IR-induced activation of both NF-κB and p53 in murine Atm-deficient tissues and in cell lines derived from A-T patients (Banin *et al*., 1998; Piret *et al*., 1999; Li *et al*., 2001; Saito *et al*., 2002). Focusing on the putative NF-κB-mediated arm, our analysis points to several novel direct targets of this TF and demonstrates the power of combining computational promoter analysis and gene expression data in elucidating intricate transcriptional networks. Using EMSA, we biochemically validated the Atm dependence of the IR-induced enhancement in DNA binding activity of NF-κB in the lymphoid cells. Thus, our approach was able to dissect two major arms in the Atm-mediated transcriptional response, according to the transcriptional regulators that function downstream of Atm.

Importantly, the Atm-dependent response contained several p53-direct targets with major proapoptotic role, as well as several NF-κB-direct targets with antiapoptotic function. Taken together, our findings suggest a model in which, in the response of lymphoid cells to IR, pro-, and antiapoptotic signals are induced in parallel, the former being mediated by NF-κB and the latter by p53, and the activation of both being Atm-dependent. An antiapoptotic role of NF-κB was reported in many different cellular systems, and its activation was linked to cellular resistance to apoptosis induced by radiation and chemotherapeutic treatment in several cancers (reviewed in (Garg and Aggarwal, 2002)). However, in addition to the more common antiapoptotic role, NF-κB was also reported to play a proapoptotic role under several biological conditions (Abbadie *et al*., 1993; Qin *et al*., 1999; Schneider *et al*., 1999). The opposing effects of NF-κB probably reflect cell type-specific function of this signaling pathway, and/or dependency of its outcome on the inducing signal (Shishodia and Aggarwal, 2004).

In Stankovic *et al*.'s (2004) study on the IR response of B-Cll cells with various ATM and p53 genotypes, they reported parallel induction of proapoptotic ATM- and p53-dependent transcriptional response, and ATM-dependent, p53-independent prosurvival response. Our findings point to NF-κB as the missing piece in the puzzle, that is, as the major regulator downstream to ATM that mediates the antiapoptotic arm in lymphoid cells. Indeed, very recently, Weston *et al*. (2004) showed that increased NF-κB survival signaling endows acute lymphoblastic leukemia tumors with resistance to IR-induced apoptosis. However, a model that depicts the ATM-p53 and ATM-NF-κB pathways as parallel, linear and independent is probably over-simplified. Accumulating data derived from several cell types suggest that the p53- and NF-κB-mediated arms maintain multiple cross-talks (Wu and Lozano, 1994; Ryan *et al*., 2000; Tergaonkar *et al*., 2002; Ding *et al*., 2003), indicating that the logic of the IR-induced response network and the balance between apoptotic and survival signals are highly intricate and dependent on cellular context.

The mechanisms by which ATM activates and stabilizes p53 are well-established. ATM directly phosphorylates p53, as well as its inhibitor and E3 ubiquitin ligase, Mdm2, and the checkpoint kinase Chk2, which in its turn phosphorylates p53 on yet another site (reviewed by (Shiloh, 2003; Kurz and Lees-Miller, 2004)). All these modifications contribute to the stabilization and rapid accumulation of p53 in response to IR-induced DNA damage. On the other hand, the mechanisms by which ATM activates the NF-κB pathway remain elusive. Li *et al*. (2001) demonstrated that ATM is required for the DSB-induced activation of the NF-κB pathway, including activation of the IKK complex that phosphorylates NF-κB's inhibitor, thereby leading to its degradation. Recently, Hur *et al*. (2003) reported the death domain kinase RIP to be an essential component upstream to IKK in the activation of NF-κB by DNA damage. Importantly, RIP was demonstrated to physically interact with IKK upon exposure of cells to DNA damaging agents, and this interaction was ATM-dependent. The direct substrate(s) of ATM in this signaling pathway, and how the alarm signal is propagated from the nucleus to the cytoplasm remain to be determined. A recent study pointed to IKBKG (NEMO/IKKγ) subunit of the IKK complex, which shuttles between the nucleus and the cytoplasm, as a key player in the transmission of the signal (Huang *et al*., 2003).

In previous work, we demonstrated that *in silico* dissection of transcriptional networks is feasible in the analysis of gene expression data obtained from a homogenous, synchronized population of culture cells (Elkon *et al*., 2003). Here, we demonstrate that this functional genomics approach is sensitive enough to dissect transcriptional networks in a more physiological relevant situation – a mixture of cells in the tissue of an irradiated animal. Our findings elucidate novel aspects of the Atm-dependent transcriptional network induced by IR in lymphoid tissues, point to novel putative NF-κB targets, and suggest a mechanistic model for cellular balancing between pro- and antiapoptotic signals in response to genotoxic stress. The model that emerges has implications for tailoring rational therapeutic strategies for management of cancers of lymphoid origin. It suggests that a combined treatment that restores the p53-mediated apoptotic arm while blocking the NF-κB-mediated prosurvival arm could effectively increase the radiosensitivity of lymphoid tumors.

Materials and methods

Animals and radiation treatment
Male Atm+/+ and Atm−/− SV129 mice at the age of 5–7 weeks were irradiated at a total dose of 15 Gy using a Clinac 600C accelerator (Varian Medical Systems, Inc.). Lymph node tissues were obtained from untreated and irradiated animals at two time points, 30 and 120 min postirradiation, and were immediately snap-frozen in liquid nitrogen.

RNA isolation
Total RNA was isolated from frozen tissues using TRIzol reagent (Life Technologies) and treated with DNaseI (DNA freeTM, Ambion). RNA was then purified using PLG tubes (Eppendorf) and phenol/chloroform extraction, ethanol-precipitated and quantitated. The integrity of the RNA and the absence of larger amounts of contaminating genomic DNA were checked by gel electrophoresis.

Target preparation and chip hybridization
Preparation of samples for hybridization and microarray processing were carried out according to Affymetrix standard protocols. Affymetrix GeneChip MGU74Av2 arrays were used in this study. Each sample represented a pool of tissues from three animals. Samples from untreated mice were probed in independent hybridization triplicates, and samples from irradiated mice were probed in independent hybridization duplicates.

Data preprocessing and cluster analysis
Signal intensities were determined by Affymetrix MAS 5.0 software. All chips were scaled to an average signal intensity of 150. The entire dataset was uploaded to the GEO DB (accession number GSE2118). Probe sets that registered 'Absent' flags by MAS 5.0 in all measured conditions were excluded. Signal intensities below 40 were set to 40. A representative expression level for each probe set in each of the six tested conditions (two genotypes, three time points) was computed by averaging the probe set's signal intensities in the replicate arrays. As a filtering step, we scanned the data set for genes whose expression level varied by at least 1.75-fold over the six genotype-treatment conditions (max_level/min_level > 1.75). In all, 1206 probe sets that met this criterion were subjected to cluster analysis. Expression levels for each probe set were normalized to mean = 0 and variance = 1 over the six conditions. Cluster analysis was performed using the CLICK algorithm (Sharan and Shamir, 2000) with a homogeneity parameter value of 0.75. CLICK was executed via EXPANDER analysis package (http://www.cs.tau.ac.il/~rshamir/expander/expander.html).

Functional categories analysis
Association of mouse genes with Gene Ontology (GO) biological processes' categories is provided by the MGI and was downloaded from the GO web site (http://www.geneontology.org/doc/GO.current.annotations.html). The statistical significance of the enrichment of specific clusters for genes of a particular functional category was determined by computing the upper tail of the hypergeometric distribution (see, for example, (Tavazoie *et al*., 1999)), taking into account the number of genes represented on the chip that are associated with this functional category. Certain genes were represented in the microarray by several probe sets. To avoid biases, each gene was counted only once.

Computational promoter analysis
Putative promoter sequences corresponding to all known murine and human genes were extracted from the mouse and human genome sequence, respectively, using a Perl script based on the application programming interface developed by the Ensembl project (v13, May 2003 release) (Clamp *et al*., 2003). For each gene flagged as a 'known gene', a genomic sequence was extracted, spanning from 1000 bp upstream to 200 bp downstream of the gene's putative transcription start site (TSS). A total of 16 542 and 19 565 putative promoters were extracted for mouse and human, respectively. We applied the PRIMA program in an attempt to identify TFs that possibly control the observed transcriptional modulation in our microarray dataset. The PRIMA program is described in (Elkon *et al*., 2003) and can be downloaded from http://www.cs.tau.ac.il/~rshamir/prima/PRIMA.htm. In short, given *target* and *background* sets of promoters, PRIMA performs statistical tests to identify TFs whose binding sites are significantly over-represented in the target set relative to the background set. In this study, each gene cluster was considered a target set. The entire collection of putative murine promoters described above was used as the background set. Binding sites that are recognized and bound by TFs were modeled by position weight matrices (PWMs). PWMs that represent mammalian TF binding sites were obtained from the TRANSFAC database (Matys *et al*., 2003). In the analysis, both strands of each promoter were scanned for putative binding sites. Similarity scores between a subsequence and a PWM are computed by PRIMA as described in (Elkon *et al*., 2003) with the modification that each column in the PWM is weighted by its information content. The enrichments identified by PRIMA in this study were robust as they remained stable over a large range of threshold values. For all PWMs except p53, we report results from runs in which we set the parameter fpRate to 100 (corresponding to an average of one hit per 10 000 bp in random sequences). The results we report for p53 are from a run with fpRate = 50 (corresponding to an average of one hit per 20 000 bp in random sequences) in order increase the specificity of the reported putative targets. (The runs with fpRate values of 50 and 100 gave comparable statistical enrichment for p53.)

Quantitative real-time RT–PCR
Total RNA (5 μg) were used for cDNA synthesis by oligo(dT) and SuperScript™ II RNase H^- reverse transcriptase (Life Technologies). Quantitative Real-time PCR using SYBR® Green PCR master mix (Applied Biosystems, Foster City, CA, USA) was performed with ABI PRISM 7900HT sequence detection system (Applied Biosystems). The comparative Ct method was employed for quantification of transcripts according to the manufacturer's protocol. Measurement of delta Ct was performed in triplicate. Primers used in the RT–PCR assays are provided as Supplementary Table D. Each of the 11 selected genes was assayed in four RNA samples: Atm+/+ and Atm−/− tissues prior to irradiation, and 120 min post IR. All the assays were carried out in triplicates, and two to three independent experiments were performed to verify the reproducibility of the results. The results were normalized against GAPDH expression in each of the samples.

Nuclear extracts and electrophoretic mobility shift assays (EMSA)
Lymph node tissues were washed with ice-cold phosphate-buffered saline and maintained in 0.32 M sucrose. The organs were homogenized in ice-cold hypotonic buffer A (0.5 M sucrose, 10 mM Tris-HCl pH 7.9, 1.5 mM MgCl2, 10%

glycerol, 1 mM EDTA, 1 mM DTT, 1 mM PMSF, protease inhibitor cocktail (Boehringer Manheim), 0.2 mM $NaVO_3$ (500 μl)). The lysates were left on ice for 15 min and centrifuged for 10 min at 7500 *g*. The supernatants (cytoplasmic extracts) were removed and the nuclear pellets were rinsed once with ice-cold buffer A and resuspended in buffer B (0.42 M NaCl, 20 mM Tris-HCl pH 7.9, 25% glycerol, 0.2 mM EDTA, 1 mM DTT and protease inhibitor cocktail (Boehringer Manheim), 0.2 mM $NaVO_3$, (100 μl)). The nuclear extracts were incubated for 45 min on ice and centrifuged for 20 min at 15 500 *g*; the supernatants were collected and used for electrophoretic mobility shift assay (EMSA). The binding reaction mixture containing 10 mM Tris-HCl (pH 7.9), 60 mM KCl, 0.4 mM dithiothreitol, 10% glycerol, 2 μg of bovine serum albumin, 1 μg of poly(dI-dC), 15 000 c.p.m. of ^{32}P-labeled NF-κB oligonucleotides (5′-AGTTGAGGGGACTTTCCCAGGC-3′) (Santa-Cruz Biotechnology) was incubated for 30 min with 8 μg of nuclear extract. To confirm that the bands detected in the EMSA assays were specific to NF-κB, we repeated these assays in the presence of a 100-fold excess of unlabeled NF-κB binding oligonucleotides. All bands were indeed significantly reduced under this condition, indicating that they were NF-κB specific. Products were analysed on a 5% acrylamide gel made up in 1 × TGE (50 mM Tris, 400 mM glycine, 2 mM EDTA). Dried gels were exposed to X-ray film or to phosphor screen (Molecular Dynamics). Quantitative data were obtained using phosphoimager analysis (Molecular Dynamics).

Acknowledgements

We thank Nir Orlev for assistence in the manuscript preparation. This study was supported by research grants from the A-T Children's Project, the Ministry of Science and Technology, Israel, The A-T Medical Research Foundation, and the Israel Science Foundation. R Elkon is a Joseph Sassoon Fellow. This work was carried out in partial fulfillment of the requirements for the PhD degrees of S Rashi-Elkeles and R Elkon.

References

Abbadie C, Kabrun N, Bouali F, Smardova J, Stehelin D, Vandenbunder B *et al*. (1993). *Cell* **75**: 899–912.
Ashburner M, Ball CA, Blake JA, Botstein D, Butler H, Cherry JM *et al*. (2000). *Nat Genet* **25**: 25–29.
Bakkenist CJ, Kastan MB. (2004). *Cell* **118**: 9–17.
Banin S, Moyal L, Shieh S, Taya Y, Anderson CW, Chessa L *et al*. (1998). *Science* **281**: 1674–1677.
Chun HH, Gatti RA. (2004). *DNA Repair (Amsterdam)* **3**: 1187–1196.
Clamp M, Andrews D, Barker D, Bevan P, Cameron G, Chen Y *et al*. (2003). *Nucleic Acids Res* **31**: 38–42.
Deveraux QL, Reed JC. (1999). *Genes Dev* **13**: 239–252.
Ding GR, Honda N, Nakahara T, Tian F, Yoshida M, Hirose H *et al*. (2003). *Radiat Res* **160**: 232–237.
el-Deiry WS, Kern SE, Pietenpol JA, Kinzler KW, Vogelstein B. (1992). *Nat Genet* **1**: 45–49.
Elkon R, Linhart C, Sharan R, Shamir R, Shiloh Y. (2003). *Genome Res* **13**: 773–780.
Garg A, Aggarwal BB. (2002). *Leukemia* **16**: 1053–1068.
Gasch AP, Huang M, Metzner S, Botstein D, Elledge SJ, Brown PO. (2001). *Mol Biol Cell* **12**: 2987–3003.
He KL, Ting AT. (2002). *Mol Cell Biol* **22**: 6034–6045.
Huang TT, Wuerzberger-Davis SM, Wu ZH, Miyamoto S. (2003). *Cell* **115**: 565–576.
Hur GM, Lewis J, Yang Q, Lin Y, Nakano H, Nedospasov S *et al*. (2003). *Genes Dev* **17**: 873–882.
Jelinsky SA, Estep P, Church GM, Samson LD. (2000). *Mol Cell Biol* **20**: 8157–8167.
Jelinsky SA, Samson LD. (1999). *Proc Natl Acad Sci USA* **96**: 1486–1491.
Kurz EU, Lees-Miller SP. (2004). *DNA Repair (Amsterdam)* **3**: 889–900.
Li N, Banin S, Ouyang H, Li GC, Courtois G, Shiloh Y *et al*. (2001). *J Biol Chem* **276**: 8898–8903.
Lockhart DJ, Winzeler EA. (2000). *Nature* **405**: 827–836.
Matys V, Fricke E, Geffers R, Gossling E, Haubrock M, Hehl R *et al*. (2003). *Nucleic Acids Res* **31**: 374–378.
Miyashita T, Reed JC. (1995). *Cell* **80**: 293–299.
Pettitt AR, Sherrington PD, Stewart G, Cawley JC, Taylor AM, Stankovic T. (2001). *Blood* **98**: 814–822.
Piret B, Schoonbroodt S, Piette J. (1999). *Oncogene* **18**: 2261–2271.
Qin ZH, Chen RW, Wang Y, Nakai M, Chuang DM, Chase TN. (1999). *J Neurosci* **19**: 4023–4033.
Robles AI, Bemmels NA, Foraker AB, Harris CC. (2001). *Cancer Res* **61**: 6660–6664.
Ryan KM, Ernst MK, Rice NR, Vousden KH. (2000). *Nature* **404**: 892–897.
Saito S, Goodarzi AA, Higashimoto Y, Noda Y, Lees-Miller SP, Appella E *et al*. (2002). *J Biol Chem* **277**: 12491–12494.
Schneider A, Martin-Villalba A, Weih F, Vogel J, Wirth T, Schwaninger M. (1999). *Nat Med* **5**: 554–559.
Sharan R, Shamir R. (2000). *Proc Int Conf Intell Syst Mol Biol* **8**: 307–316.
Shiloh Y. (2003). *Nat Rev Cancer* **3**: 155–168.
Shiloh Y, Kastan MB. (2001). *Adv Cancer Res* **83**: 209–254.
Shishodia S, Aggarwal BB. (2004). *Biochem Pharmacol* **68**: 1071–1080.
Stankovic T, Hubank M, Cronin D, Stewart GS, Fletcher D, Bignell CR *et al*. (2004). *Blood* **103**: 291–300.
Stankovic T, Stewart GS, Byrd P, Fegan C, Moss PA, Taylor AM. (2002a). *Leuk Lymphoma* **43**: 1563–1571.
Stankovic T, Stewart GS, Fegan C, Biggs P, Last J, Byrd PJ *et al*. (2002b). *Blood* **99**: 300–309.
Tavazoie S, Hughes JD, Campbell MJ, Cho RJ, Church GM. (1999). *Nat Genet* **22**: 281–285.
Tergaonkar V, Pando M, Vafa O, Wahl G, Verma I. (2002). *Cancer Cell* **1**: 493–503.
Wang CY, Mayo MW, Korneluk RG, Goeddel DV, Baldwin Jr AS. (1998). *Science* **281**: 1680–1683.
Weston VJ, Austen B, Wei W, Marston E, Alvi A, Lawson S *et al*. (2004). *Blood* **104**: 1465–1473.
Wu H, Lozano G. (1994). *J Biol Chem* **269**: 20067–20074.

Supplementary Information accompanies the paper on Oncogene website (http://www.nature.com/onc)